Theoretical analysis and experiments of axial flux pm motors with minimized cogging torque [†]

Dong Ho Kim[1], Jong Hyun Choi[2], Chang Woo Son[3] and Yoon Su Baek[2]*

[1]*Department of Automation and Robots, Kyonggi Institute of Technology, Shihung, Gyeonggi, 429-792, Korea*
[2]*Department of Mechanical Engineering, Yonsei University, Seoul, 120-749, Korea*
[3]*Digital Appliance Laboratory, CTO Division, LG Electronics, Seoul, 153-802, Korea*

Abstract

This paper deals with analysis and experiments of an axial flux PM (AFPM) brushless dc motor with minimized cogging torque. Recently, many optimal designs for the AFPM motor have been done by finite element (FE) analysis, but such analysis is time-consuming. In this study, the equation of magnetic flux lines existing between PMs and core is assumed mathematically and the minimum cogging torque is calculated theoretically and geometrically without FE analysis. The form of equation is assumed to be a 2nd order polynomial. The skew angle that makes the cogging torque minimized is calculated theoretically, and the value of minimum cogging torque is compared with the results obtained by FE analysis and experiments. The maximum cogging torque of a proposed AFPM motor has the smallest value approximately at a skew angle of 4° in both the theoretical and FE analysis. Compared with the non-skewed motor, the cogging torque of the skewed motor can be decreased to over 90%, which has a value of 5% of the rated torque. Two types of stator cores, with the skew angle of 0° and 4°, are analyzed, manufactured, and tested experimentally.

Keywords: Axial flux permanent magnet motor; Cogging torque; Magnetic flux; Skew angle

---

1. Introduction

For direct drive applications with high performance, many types of actuators using permanent magnets (PMs) and ferromagnetic cores have been proposed and developed. Among them, an axial flux PM (AFPM) brushless dc (BLDC) motors composed of a rotor to which an axially polarized magnet array is attached and stator including ferromagnetic core have significant advantages over conventional PM motors, such as high torque-to-weight ratio, high efficiency, adjustable air gap, and so on [1]. An AFPM motor can be suitable for direct drive applications such as electric motors of hybrid electric vehicles or hydrogen fuel cell vehicles, in-wheel electric motors, and wind genera-

tors [2-4].

Generally, the torque quality of AFPM motors is directly related to the pulsating torque, which consists of two components: cogging torque and torque ripple [5-7]. The former arises from the variation of the magnetic permeance of the stator teeth and the slots above the PMs, and the latter occurs because of fluctuations of the field distribution and the armature magneto-motive force (MMF).

In general, techniques of minimizing cogging torque to improve torque quality can be classified into two major categories. The first one includes the techniques for modifying motor design so that the pulsating torque component is minimized and smooth torque is achieved. The second way is based upon control schemes for modifying the stator excitation waveform to obtain smooth torque [8]. Caricchi et al. and Aydin et al. have reported that skewing the PMs with optimum skew angle is an effective tool for minimizing

the pulsating torque component in AFPM motors [9-10]. However, they generally use finite element (FE) analysis, which is time consuming and difficult to apply to iterative design procedures such as optimal design. Recently, Choi expressed the equation of magnetic flux lines existing between PMs and iron cores mathematically without FE analysis and calculated the detent force in the PM linear synchronous motor theoretically with several parameter changes [11]. This method may be a new, effective means in theoretical analysis of AFPM motors.

In this paper, flux density distribution is described analytically and cogging torque and thrust torque are calculated theoretically and geometrically without FE analysis. Therefore, the analytical model representing the cogging torque as the function of geometric parameters of the motor is developed. Consequently, cogging torque can be obtained by applying the solved flux line equation and the flux density equation to the Lorentz force equation by using the Maxwell stress tensor.

2. Axial flux permanent magnet motor

Fig. 1 shows the assembly view of the proposed AFPM motor with an iron core. Several pairs of windings are arranged on the stator alternately and the rotor on which several PMs are attached is assembled with the stator. In this paper, the proposed AFPM motor has 16 magnets in the rotor and 24 teeth in the stator.

2.1 Theoretical approach of electromagnetic field

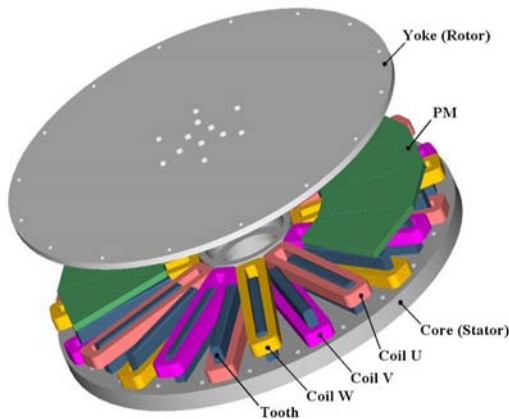Fig. 2 shows the side view of the analytical model. τ, w, h_m and g are the pole pitch, magnet width, mag-

net thickness and air gap length, respectively. In order to simplify the model, the following assumptions are made.

(1) All layers extend to infinity in the $\pm x$-direction.

(2) Variations in the y-direction are ignored and vector potential can be a function of x and z but y-direction.

(3) The relative permeability of the iron yoke is infinite.

(4) The physical constants of the layers are homogeneous, isotropic, and linear.

Distribution equations of electromagnetic system can be expressed by using Maxwell's equations, Ohm's law, and magnetic vector potential **A** defined as $\nabla \times \mathbf{A} = \mathbf{B}$. Their solutions have been well studied in other researches [12-13]. Therefore, we briefly discuss the theoretical results for the magnetic field distributions of the system. Equation (1) is the governing equation of the electromagnetic systems, which is expressed as the partial differential equation for the magnetic vector potential **A**.

$$\nabla^2 \mathbf{A} = \mu_0 \sigma \left[\partial \mathbf{A} / \partial t - \mathbf{v} \times (\nabla \times \mathbf{A}) \right] - \mu_0 \nabla \times \mathbf{M} \quad (1)$$

In Eq. (1), $\mu_0 \, (= 4\pi \times 10^{-7} \, (N/A^2))$ is the permeability of the free space, σ is the electrical conductivity $((\Omega\text{-m})^{-1})$ of medium, **v** is the moving velocity (m/sec) of the medium and **M** is magnetization vector field (A/m) expressed from Fourier series as

$$\mathbf{M} = \sum_{n=1,3,5\cdots}^{\infty} M_p \, e^{j(\omega t - \beta x)} \hat{k} \quad (2)$$

where $M_p = 4M \sin(\beta w / 2) / n\pi$, $\beta = n\pi / \tau$, and ω means electrical angular velocity (rad/s).

In the air gap, electrical conductivity and magnetization vector field are zero, and therefore, the governing equation can be expressed as

$$\nabla^2 \mathbf{A}_{II} = 0 \quad (3)$$

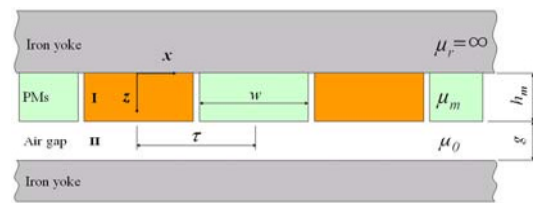where subscript *II* represents the layer of air gap. The

Fig. 1. Schematic design of a proposed AFPM motor.

Fig. 2. Geometric modeling for theoretical analysis.

x- and *z*-directional flux density distributions in the air gap are calculated by using the following equations:

$$\mathbf{B} = \nabla \times \mathbf{A} \tag{4}$$
$$= (\partial A_{II} / \partial z)\, \hat{i} - (\partial A_{II} / \partial x)\, \hat{k} = B_{x,II}\, \hat{i} + B_{z,II}\, \hat{k}$$

$$B_{x,II} = \partial A_{II} / \partial z \tag{5}$$
$$= \sum_{n=1,3,5\cdots}^{\infty} \left\{ \frac{je^{-\beta(g+h_m)}(-1+e^{2\beta g})(-1+e^{2\beta h_m})\mu_0^{\,2}M_p}{4(\Lambda+\Delta)} \right\} e^{j(\omega t - \beta x)}$$

$$B_{z,II} = -\partial A_{II} / \partial x \tag{6}$$
$$= \sum_{n=1,3,5\cdots}^{\infty} \left\{ \frac{e^{-\beta(g+h_m)}(1+e^{2\beta g})(-1+e^{2\beta h_m})\mu_0^{\,2}M_p}{4(\Lambda+\Delta)} \right\} e^{j(\omega t - \beta x)}$$

where $\Lambda = \mu_m \cosh\beta h_m \sinh\beta g$, $\Delta = \mu_0 \cosh\beta g \sinh\beta h_m$ and $\hat{i}$ and $\hat{k}$ mean *x*- and *z*-axis unit vectors, respectively.

The torque intensity of the motor depends on the value of current density in the stator windings and magnetic flux density B_z produced by PMs in the air gap. The torque, **T** can be computed theoretically as follows:

$$\mathbf{T} = r \times \mathbf{F} = r \times \int I(dl \times \mathbf{B}) \tag{7}$$

where **F** is the thrust force produced by windings and PMs, *r* is a radius of rotation and *I* is the value of total current passing through the air gap.

2.2 Equation of flux lines

In this paper, the shape of flux lines is supposed to be an equation of a 2nd order polynomial [11]. The pattern of flux, the coordinate, and the shape of flux at the side of core are described in Fig. 3. As shown in the figure, l_i represents i^{th} flux line length from the intersection $\tilde{x}_{0i}$ to the intersection $\tilde{z}_{0i}$ and the total length of flux lines, therefore, can be calculated as follows as Eq. (8).

$$\sum_{i=1,2,3\cdots} l_i = \sum_{i=1,2,3\cdots} \sum_{j=1,2,3\cdots} \sqrt{(\tilde{z}_{i,j+1}-\tilde{z}_{i,j})^2 + (\tilde{x}_{i,j+1}-\tilde{x}_{i,j})^2} \tag{8}$$

where subscript *j* is the index number going along with l_i. The equation of flux lines is expressed as follows:

$$\tilde{z} = a\tilde{x}^2 - \tilde{z}_{0i} \tag{9}$$

where coefficient a can be solved from boundary condition expressed in Eq. (10), and therefore, the equation of flux lines can be calculated as Eq. (11) .

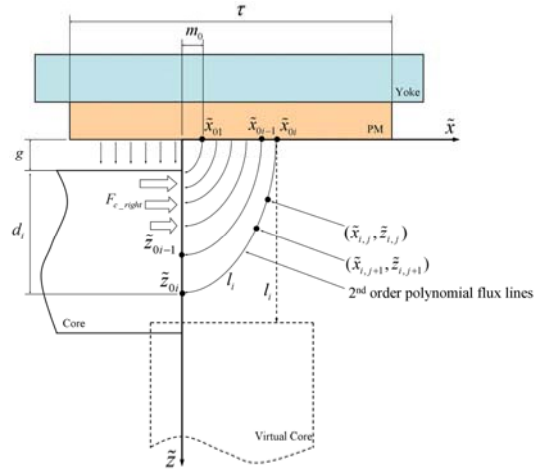$$\tilde{z}\big|_{\tilde{x}=\tilde{x}_{0i}} = 0 \tag{10}$$

Fig. 3. 2nd order polynomial flux lines, virtual flux and cogging torque expressed in analytical model.

$$\tilde{z} = a\tilde{x}^2 - \tilde{z}_{0i} = \frac{\tilde{z}_{0i}}{\tilde{x}_{0i}^2}\tilde{x}^2 - \tilde{z}_{0i} = \frac{\tilde{z}_{0i}}{\tilde{x}_{0i}^2}\tilde{x}^2 - g - d_i \tag{11}$$

where d_i is the distance from the surface of the core to the point of $\tilde{z}_{0i}$, and that is an important factor to be desired for solving the cogging torque analytically [11].

2.3 Theoretical analysis of cogging torque

From the Lorentz force equation, the force on a charge for the unit volume can be expressed as

$$\mathbf{F} = \rho\mathbf{E} + \mathbf{J} \times \mathbf{B} \tag{12}$$

where ρ is electric charge density, **E** is electric field, and **J** is current density. It can be expressed by using the Maxwell stress tensor as

$$T_{ij} \equiv \varepsilon_0 \left(E_i E_j - \frac{1}{2}\delta_{ij}E^2 \right) + \frac{1}{\mu_0} \left(B_i B_j - \frac{1}{2}\delta_{ij}B^2 \right) \tag{13}$$

where δ_{ij} means Kronecker delta and subscript *i, j* indicate the coordinates; thus, T$_{ij}$ means the *i* axis tensor toward the *j* direction. Therefore, the magnetic attraction force can be expressed as follows:

$$F_{attraction} = -d\tau \left(\left|B_z\right|^2 - \left|B_x\right|^2 \right) / 2\mu_0 \tag{14}$$

where *d* means *y*-directional depth of PM and the sign of minus means that the attraction force goes toward the PMs. In Fig. 3, the conversion of attraction force to cogging torque is expressed graphically. Suppose that the bending flux line from point ($\tilde{x}_{0i}$,0) to point $(0, \tilde{z}_{0i})$ is equal in length with the dotted virtual flux

line extending straight, the virtual core in the figure seems to be attracted to the PMs vertically. The magnitude of attraction can be calculated from Eq. (14) and the force can be converted to the drag force on the right side of core at the point of $(0, \tilde{z}_{0i})$. The x- and z-directional flux density distributions in the air gap of virtual flux can be solved by using Eqs. (5) and (6) and the attraction force solved in Eq. (14), which is considered to be the cogging torque of the core as shown in Eq. (15)

$$F_{c\_right} = d\tau \left(|B_z|^2 - |B_x|^2 \right) / 2\mu_0 \tag{15}$$

where F_{c_right} means the cogging torque acting on the right side of core to the direction of $\tilde{x}$ axis.

2.4 FE analysis of cogging torque

In this paper, the FE analytical tool MAX-WELL® ver.10 numerically calculates the magnetic field of the 3-D motor configuration. The FE mesh is automatically generated for the calculation of magnetic flux, flux density, and torque distributions. The boundary of the FE model is surrounded by air with enough thickness. In next chapter, both the continuous torque and the pulsating torque due to the cogging torque are computed by the theoretical and FE analysis and the results are compared with each other.

3. Comparison of theoretical and FE analysis

For the proposed AFPM motor, the number of poles and slots is set in a ratio of 2:3, that is, a 16-pole rotor and 24-slot stator are assembled with each other.

3.1 Cogging torque and continuous torque

In order to reduce the cogging torque of AFPM motors with a ferromagnetic core, it is useful to skew either stator slots or rotor magnets. In this paper, the skewing of stator slots is considered and skew angle α is defined as the relative angle between the teeth of the core and PMs as depicted in Fig. 4. Namely, when the angle of a core tooth is equal to that of a PM, the skew angle α is zero. The range of variation in skew angle is limited by the structural topology of PMs and core teeth. Both of the limited values of skew angles are from $\alpha = -3.75°$ to $\alpha = 6.75°$.

In Fig. 5, the relationship between skew angle and the absolute maximum cogging torque is expressed, and the results of theoretical and FE analytical cogging torque are compared with each other. As shown in the
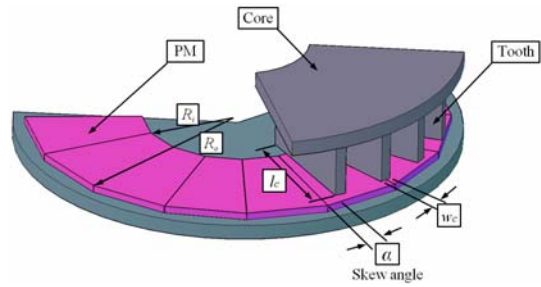

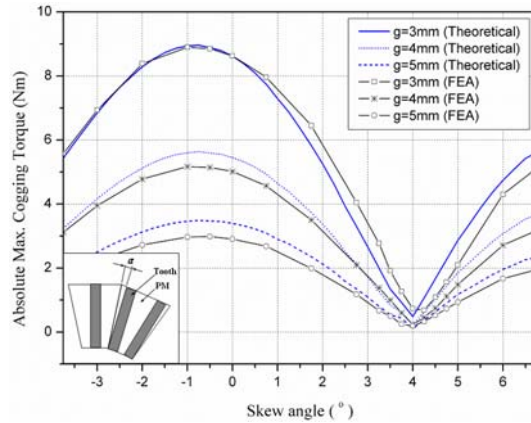Fig. 4. Skew angle and design parameters related to core tooth and PM.

Fig. 5. Absolute maximum cogging torque according to skew angle α.

figure, the maximum cogging torque has the smallest value approximately at the angle of 4° and the largest value near the angle of −1° in both analyses. As the air gap increases, the values of the maximum cogging torque diminish remarkably and its curve has a gentle slope. Two analytical results showed good agreement and a skew angle of 4° can minimize the cogging torque.

Fig. 6 shows the theoretical and FE analytical cogging torques with several air gaps according to the rotor position. The cogging torque of skewed and non-skewed motor is illustrated in Fig. 6(a) and 6(b), respectively, at 3, 4, and 5mm air gaps. As shown in the figure, the cogging torque of the non-skewed motor is much bigger than that of the skewed motor.

Gross continuous torque, including the cogging torque, is depicted in Fig. 7 according to the rotor position. As shown in Fig. 7(a), the torque of the non-skewed motor fluctuates excessively as rotor position changes because the non-skewed motor produces large oscillating cogging torque to a great extent as shown
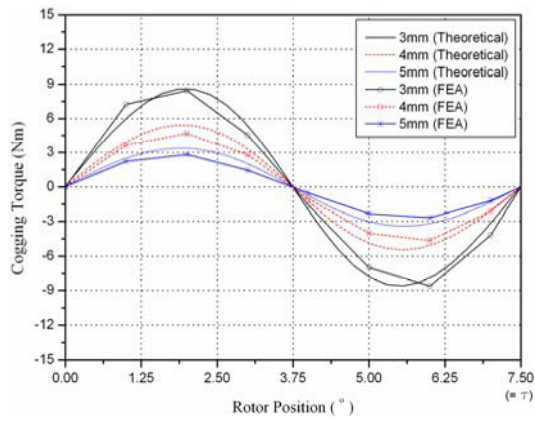
(a)
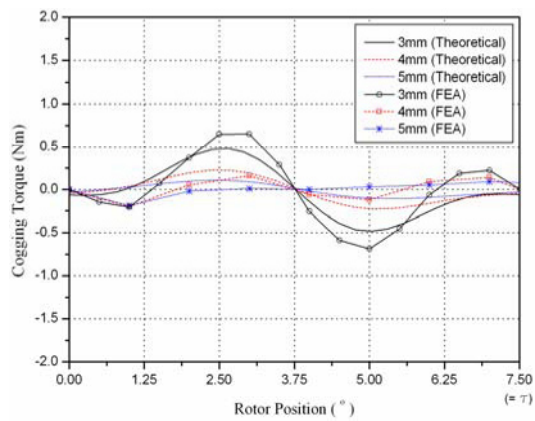
(b)

Fig. 6. Theoretical and FE analytical cogging torque according to rotor position: (a) non-skewed ($\alpha = 0°$) motor and (b) skewed ($\alpha = 4°$) motor.

### 3.2 Length-to-Width ratio of tooth, ξ

The shape of the core tooth is closely related to the magnitude of cogging torque, and thus, the skew angle made by tooth shape is to be the main design parameter to minimize the cogging torque. Besides this skew angle, another design parameter to configure a plane section of a core tooth is involved, and this parameter also affects the determination of minimized cogging torque. Accordingly, a new parameter, which is length-to-width ratio ξ at a core tooth, is introduced and defined by $\xi = \ell_c / w_c$. The design parameter

Table 1. Change of core dimensions: overall size change (constant $\xi = 9.375$).

Design parameter (mm)	Ref.	50% Dec.	25% Dec.	25% Inc.	50% Inc.
Inner radius, R_i	48	24	36	60	72
Tooth width, w_c	6.4	3.2	4.8	8	9.6
Tooth length, ℓ_c	60	30	45	75	90
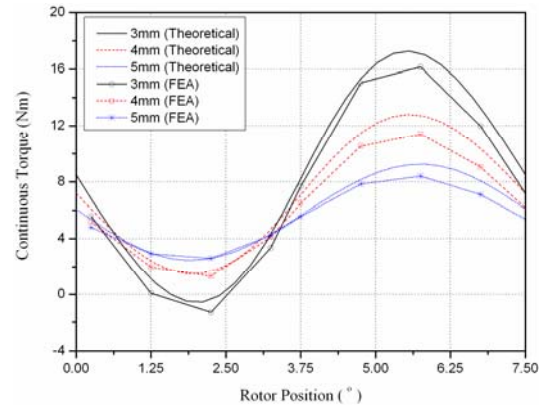
(a)
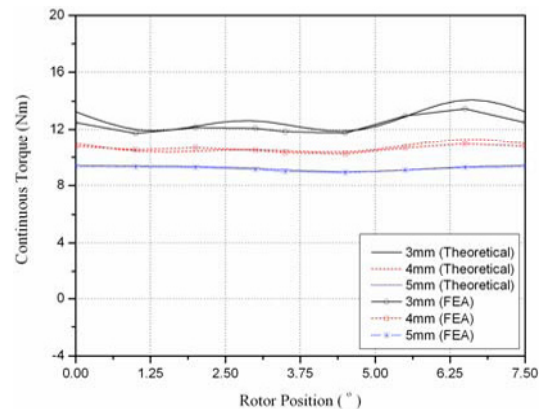
(b)

Fig. 7. Theoretical and FE analytical continuous torque according to rotor position: (a) non-skewed ($\alpha = 0°$) motor and (b) skewed ($\alpha = 4°$) motor.

in Fig. 6(a). On the other hand, the pulsation of torque existing in the skewed motor, as shown in Fig. 7(b), is relatively very small.

about four step changes is shown in Table 1. In Fig. 8, the results of theoretical and FE analytical cogging torque are compared at an air gap of 4mm. As shown in the figure, the maximum cogging torque has the smallest value at the angle of 4° or the angle of 3.75° and 4.25° near the angle of 4 ° in both analyses.
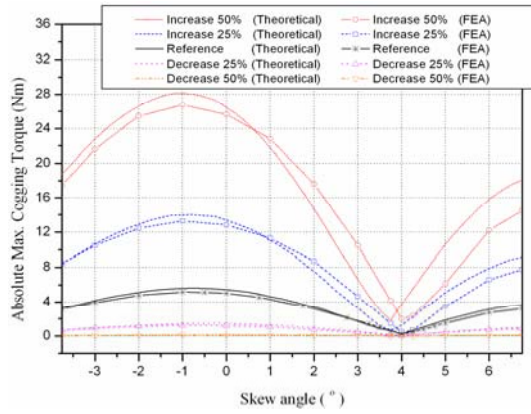
Fig. 8. Maximum cogging torque according to skew angle by overall size change (g=4mm).
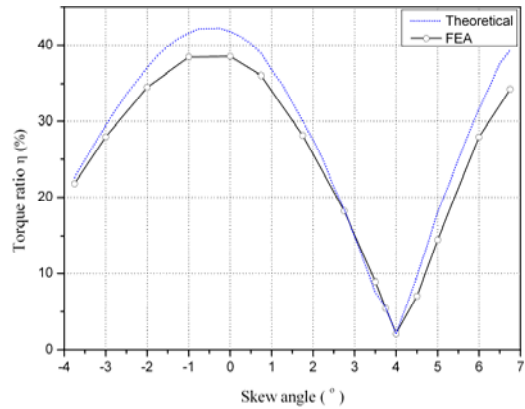

Fig. 9. Torque ratio according to skew angle at 4mm air gap in reference model.

3.3 Torque ratio, η

In order to examine the relationship of cogging torque to continuous torque, torque ratio is considered and defined by $\eta = |T_c/T_n| \times 100 \ (\%)$, where T_c is absolute maximum cogging torque and T_n is mean continuous torque. Fig. 9 represents the torque ratio according to skew angle at 4mm air gap in the reference model whose inner radius is $R_i = 48$ mm and length-to-width ratio is $\xi = 9.375$. The graph pattern is similar to that of the maximum cogging torque, and the minimum value of torque ratio is under about 3% at the skew angle of $4°$.

4. Experiment and results

Two types of stator core with skew angle 0° (Model A) and 4° (Model B), rotor with PM arrangement, and motor assembly are shown in Fig. 10 and basic dimensions and specifications of AFPM motors are shown in Table 2. An electric current in three-phase is to be supplied periodically by using the PWM method from the motor driver through the U-V-W coil, and is to be synchronized with pole pitch. The feedback of rotor position can be accomplished by using an encoder and the rotational motion is guided through ball bearings.

As shown in the previous section, the minimized cogging torque of the AFPM motor was obtained theoretically by skewing the stator slots, and then the result was compared with that of FE analysis. Two analyses results showed good agreement and a skew angle of 4° can minimize the cogging torque. Therefore, two kinds of prototypes with skew angle of 0° and 4° are constructed for experiment and tested.
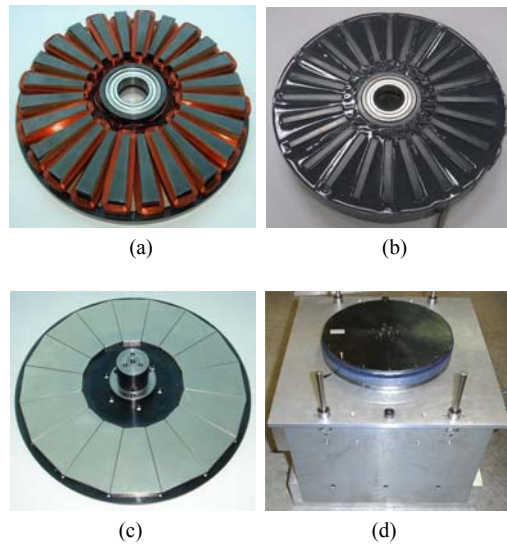

Fig. 10. Stator, rotor and assembly of AFPM motor: (a) Stator core with the skew angle of $0°$ (Model A), (b) stator core with the skew angle of $4°$ (Model B), (c) rotor with PM array, and (d) AFPM motor assembly.

Moreover, the characteristics of the two motors are compared with previously obtained analytical results.

Fig. 11 shows the cogging torque distribution of prototypes according to rotor position. With some different air gaps, the experimental results of the cogging torque are compared with theoretical ones. The shape of the experimental results is about the same as that of the theoretical trajectory at all air gaps.

Fig. 12 shows the comparison of the maximum torque between the analytical and the experimental results. The phase current is measured by using the ana-

Table 2. Dimensions and parameters of the AFPM motor.

| Part	Item	Value	Unit
Rotor	Residual Flux density of PM, B_r	1.363	T
	Pole pitch, τ	22.5	°
	Thickness of PM, h_m	4	mm
	Relative permeability, μ_m	1.099	
	Number of PM	16	ea
	Inner (Outer) radius of PM array, R_i (R_o)	48(107)	mm
Stator	Slot pitch, τ_s	15	°
	Number of slot	24	ea
	Coil diameter, ϕ	0.45	mm
	Number of turns	167	
	Phase resistance, R	0.896	Ω
Air gap	Mechanical air gap, g	3, 4 or 5	mm
Type	Model A: skew angle of 0° Model B: skew angle of 4°		
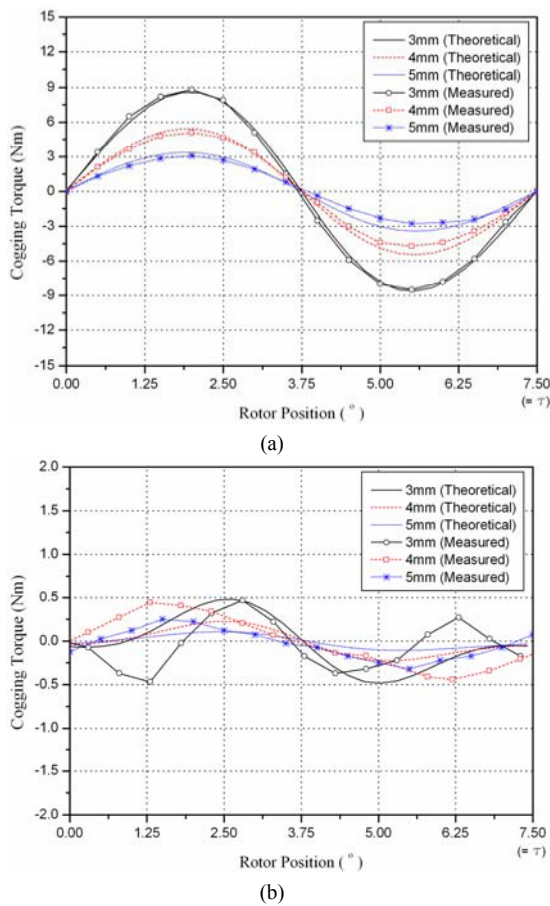
Fig. 11. Cogging torque according to rotor position: (a) non-skewed ($\alpha = 0°$) motor and (b) skewed ($\alpha = 4°$) motor.
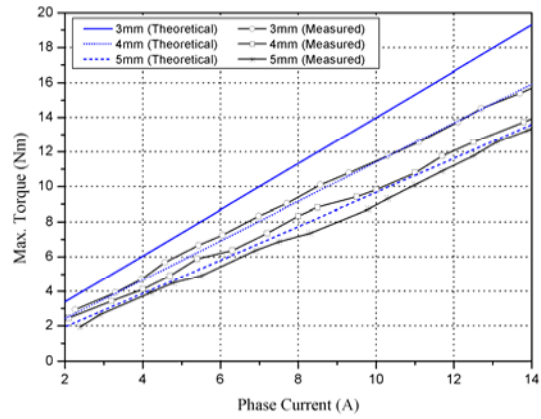

Fig. 12. Maximum torque according to phase current.

log current sensor, and the torque of the rotated rotor is obtained by means of load cell fixed to the body of the AFPM motor. The measured values of torque are smaller than the analytical ones because some parameters are neglected to simplify the modeling of the proposed AFPM motor. The flux leakage, for example, causing the attenuation of flux density at the edge of the rotor, is neglected.

5. Conclusions

AFPM BLDC motors with the minimized cogging torque are proposed. A brief overview of PM flux density, an equation of flux lines and cogging torque was provided analytically and graphically without FE analysis. The FE analytical method was merely used for comparison of the theoretical analysis. The theoretical results showed good agreement with those obtained by FE analysis; therefore, it is possible to calculate and reduce the cogging torque easily and quickly.

The optimal design of AFPM motors was performed to achieve the minimized cogging torque for different sizes of motor by skewing the stator slots. Besides the skew angle, another design parameter, length-to-width ratio ξ to configure the plane section of a core tooth was involved, and this parameter can also affect the determination of minimized cogging torque. From the analytical research, it was known that the skew angle of minimized cogging torque varies with the ratio. If the ratio is determined for AFPM motors, the skew angle for minimized cogging torque can be chosen by the relationship graph of the two parameters. It may be very useful to determine the skew angle for minimized cogging torque in industrial fields for designing different sizes of AFPM motors.

Experiments to obtain cogging and continuous torque were performed to validate the theoretical results in this paper. Two types of AFPM motors with skewed and non-skewed stators were manufactured and tested. The experimental results of cogging and continuous torque were compared with analytical ones at different air gaps. The experimental results also showed good agreement with analytical results. Compared with the non-skewed motor, the cogging torque of the skewed motor can be decreased to over 90%, and is likely to be achieved in the order of 5% of the rated torque.

In case an AFPM motor needs to be changed in its dimensions, it is possible to find the skew angle that theoretically makes the cogging torque minimized without a waste of time, and therefore, this method can be applied to the design of AFPM motors with various rotors and stators.

References

[1] Y. P. Yang, Y. P. Luh and C. H. Cheung, Design and control of axial-flux brushless DC wheel motors for electric vehicles - part I : multi objective optimal design and analysis, *IEEE Transactions on Magnetics*, 40 (4) (2004) 1873-1882.

[2] K. Rahman, N. Patel, T. Ward, J. Nagashima, F. Caricchi and F. Crescimbini, Application of direct drive wheel motor for fuel cell electric and hybrid electric vehicle propulsion system, *IEEE IAS Annual Meeting,* (2004) 1420-1426.

[3] S. C. Oh and A. Emadi, Test and simulation of axial flux-motor characteristics for hybrid electric vehicles, *IEEE Transactions on Vehicular Technology ,* 53 (3) (2004) 912-919.

[4] E. Muljadi, C. P. Butterfield and Y. Wan, Axial-flux modular permanent magnet generator with a toroidal winding for wind-turbine applications, *IEEE Trans. Ind. Appl. ,* 35 (4) (1999) 831-836.

[5] M. Aydin, S. Huang, T. A. Lipo, Torque quality and comparison of internal and external rotor axial flux surface-magnet disc machines, *IEEE Trans. Ind. Appl. ,* 53 (3) (2006) 822-830.

[6] T. M. Jahns and W. L. Soong, Pulsating torque minimization techniques for permanent magnet AC motor drives-a review, *IEEE Trans. Ind. Electron.,* 43 (2) (1996) 321-329.

[7] T. Li and G. Slemon, Reduction of cogging torque in permanent magnet motors, *IEEE Transactions on Magnetics,* 24 (6) (1988) 2901-2903.

[8] D. C. Hanselman, *Brushless Permanent-Magnet Motor Design*, McGraw-Hill, New York, (1994).

[9] F. Caricchi, F. Capponi, F. Crescimbini and L. Solero, Experimental study on reducing cogging torque and no-load power loss in axial-flux permanent magnet machines with slotted winding, *IEEE Trans. Ind. Appl.,* 40 (4) (2004) 1066-1074.

[10] M. Aydin, S. Huang and T. A. Lipo, Torque quality and comparison of internal and external rotor axial flux surface-magnet disc machines, *IEEE Trans. Ind. Appl. ,* 53(3) (2006) 822-830.

[11] J. H. Choi, *Experimental and Theoretical Analysis of Synchronous PM Planar Motor for Minimized Detent Force*, Ph.D. dissertation, Yonsei University, Korea, (2006).

[12] S. Yamamura, *Theory of Linear Induction Motors*, Second Ed., John Wiley & Sons, (1979).

[13] R. K. Wangsness, *Electromagnetic Fields*, Second Ed., John Wiley & Sons, (1986).

Dong Ho Kim received B.S. and M.S. degrees in Mechanical Engineering from Pusan National University in 1982 and 1984, respectively. He then received his Ph.D. degree from Yonsei University in 2007. Dr. Kim is currently a Professor at the Department of Automation and Robots at Kyonggi Institute of Technology in Gyeonggi, Korea. His research interests are in the area of production automation.

Jong Hyun Choi received B.S., M.S., and Ph.D. degrees in Mechanical Engineering from Yonsei University, Seoul, Korea, in 1996, 1998, and 2006, respectively. Dr. Choi is currently a post-doctor at the School of Mechanical Engineering at Yonsei University. His research interests are in the area of electromagnetic actuators and magnetic levitation system.

Chang Woo Son received a B.S. from Kyungwon University, Seoul, Korea, in 2006, and his M.S. degree from Yonsei University in 2008, all in mechanical engi-neering. He is currently a research engineer at DA Laboratory of LG Electronics in Seoul, Korea. His research interests are in the area of electromagnetic actuators.

Yoon Su Baek received B.S. and M.S. degrees from Yonsei University, Seoul, Korea, in 1979 and 1981, respectively, and M.S. and Ph.D. degrees from Oregon State University in 1986 and 1990, respectively, all in mechanical engineering. He worked for Samsung Heavy Industry Ltd. as head research engineer at Mechatronics Research Center from 1990 to 1993. Dr. Baek is currently a Professor at the School of Mechanical Engineering at Yonsei University. His research interests are motion devices and robotics, especially relating to multi-D.O.F. actuators. He is also interested in magnetic brake and levitation system.